



OPEN Health risk assessment and source tracking of heavy metal exposure from indoor settled dust in an environmentally vulnerable area of the Republic of Korea

Gihong Min¹, Daehwan Kim¹, Jihun Shin², Youngtae Choe¹, Sanghoon Lee¹, Jangwoo Lee³, Kilyong Choi⁴, Kyunghwa Sung⁵ & Wonho Yang¹✉

Accelerated urban and industrial expansion has intensified anthropogenic activities, increasing the emission and accumulation of hazardous substances in air, water, and soil. This study assessed health risks from heavy metals in indoor settled dust collected from Myodo-dong, Yeosu, Republic of Korea, by estimating exposure via inhalation, dermal contact, and ingestion, deriving protective exposure limits, and identifying emission sources using multivariate analysis. Indoor settled dust samples from 20 of 50 households showed elevated heavy metal concentrations, with zinc (Zn) having the highest mean level (4,912.01 µg/g). Ingestion was the dominant exposure route. Non-carcinogenic risks were within acceptable limits, while carcinogenic risks surpassed 1.0×10^{-6} for cadmium (Cd) and nickel (Ni). Cd risk was mainly ingestion-driven, whereas Ni posed the greatest concern through ingestion and dermal exposure. Lead (Pb) showed consistently low risk. Source identifications were analyzed using Pearson correlation, principal component analysis (PCA), and hierarchical cluster analysis (HCA), which grouped metals into three clusters, suggesting shared industrial origins. Positive matrix factorization (PMF) resolved five sources, four of which matched industrial sectors in pollutant release and transfer register (PRTR) data, including battery manufacturing, plastics, non-ferrous metal processing, and ceramics. Source 1, dominated by Cd, was not identified due to inventory gaps, but fence-line regression showed a strong correlation ($R^2 = 0.983$, $p < 0.01$) between Cd in ambient air and indoor settled dust, implicating emissions from a nearby steel facility.

Keywords Indoor settled dust, Heavy metals, Exposure limit, Risk assessment, Source tracking

The acceleration of urban and industrial development has intensified human presence and activity, which in turn has increased the release and buildup of harmful environmental agents via multiple exposure pathways, including the atmosphere, hydrosphere, and terrestrial systems¹. Urban industrialization has been increasingly identified as a key contributor to rising illness and death rates, as well as to declining life expectancy, based on accumulating scientific evidence^{2,3}. Additionally, industrial complexes that have been operating for more than 20 years are increasingly seen as key sources of environmental contamination, raising health risks among nearby residents as a result of sustained exposure to emitted heavy metals⁴.

Heavy metals are poorly eliminated through human metabolism and tend to accumulate in bones, adipose tissue, and muscles, potentially leading to organ damage and harmful effects on the cardiovascular and nervous systems^{5,6}. Compared to adults, children are more affected by indoor settled dust because they have weaker immune systems and spend the majority of their time in indoor environments such as homes and schools, which leads to higher exposure^{7,8}. Although children are generally more susceptible to the toxic effects of heavy metals due to physiological and behavioral characteristics, adults may also face chronic health risks from prolonged

¹Department of Health and Safety, Daegu Catholic University, Gyeongsan-si 38430, Republic of Korea. ²Department of Health and Safety Management, Songwon University, Gwangju 61756, Republic of Korea. ³Convergence Research Center for Big-Data, Cheminet Ltd, Seoul 08377, Republic of Korea. ⁴Department of Environmental Energy Engineering, Anyang University, Anyang-si 14028, Republic of Korea. ⁵Center of Environmental Health Monitoring, Daegu Catholic University, Gyeongsan-si 38430, Republic of Korea. ✉email: whyang@cu.ac.kr

exposure⁹. According to Somsunun et al. (2023)¹⁰, indoor dust in urbanized and industrial settings poses significant health risks across all age groups, highlighting the necessity for adult-specific exposure assessments and the development of tailored guidelines.

Heavy metal exposure from indoor settled dust primarily occurs through three main exposure routes, namely inhalation of airborne particles, dermal contact with contaminated surfaces, and unintentional ingestion¹¹. Among the three exposure routes, ingestion of indoor settled dust is considered the most significant, as it poses the highest potential health risk, encompassing both non-carcinogenic and carcinogenic effects of various heavy metals¹².

Dust containing heavy metals is generally introduced into indoor environments from outdoor sources, and the concentration of heavy metals in dust reflects both short-term and long-term human activities in the surrounding area¹³. Airborne dust can settle not only on roads (road dust) but also on various indoor and outdoor surfaces of buildings, including window frames, roofs, and windows¹⁴. Since dust particles may contain hazardous heavy metals, analyzing indoor settled dust is essential for identifying major emission sources and understanding potential exposure risks^{15,16}. Therefore, applying statistical techniques such as principal component analysis (PCA) and hierarchical cluster analysis (HCA) helps to identify the sources of heavy metal contamination and clarify their contribution to indoor settled dust composition¹⁷. In addition, positive matrix factorization (PMF) has been widely employed to extract latent sources from environmental concentration data, even in the absence of prior knowledge about emission profiles¹⁸.

Residents of Myodo-dong, Yeosu, the Republic of Korea, located in close proximity to major industrial complexes, have been reported to exhibit higher cancer incidence rates and elevated concentrations of heavy metals in biomonitoring samples compared to national averages, indicating an increased risk of adverse health effects¹⁹. This study analyzed indoor settled dust from Myodo-dong, Yeosu, the Republic of Korea, a residential area near major industrial complexes, to assess health risks from exposure to copper (Cu), manganese (Mn), cobalt (Co), zinc (Zn), chromium (Cr), lead (Pb), cadmium (Cd), and nickel (Ni) by inhalation, dermal contact, and ingestion, and to identify emission sources through multivariate analysis.

Materials and methods

Study area

The study was conducted in Myodo-dong, Yeosu-si, the Republic of Korea, a coastal residential area in the southern part of the country (Fig. 1). Figure 1a presents Yeosu-si, located in the southern coastal region of the Republic of Korea, while Fig. 1b shows Myodo-dong in the northern part of the city. Figure 1c illustrates that Myodo-dong is directly adjacent to three major industrial complexes including Gwangyang National, Yeosu National, and Yulchon, which contain large-scale petrochemical plants, steel manufacturing facilities, and other heavy industries. The study area was selected due to its close proximity to these emission sources and previous reports of elevated environmental concentrations of heavy metals. The study area was selected due to its close proximity to these emission sources and previous reports of elevated environmental concentrations of heavy metals. From a total of 50 households in Myodo-dong, 20 households that voluntarily agreed to participate were selected to ensure adequate spatial coverage. Sampling design and household selection were guided by reference to a previous national survey conducted in the same area, thereby supporting the representativeness

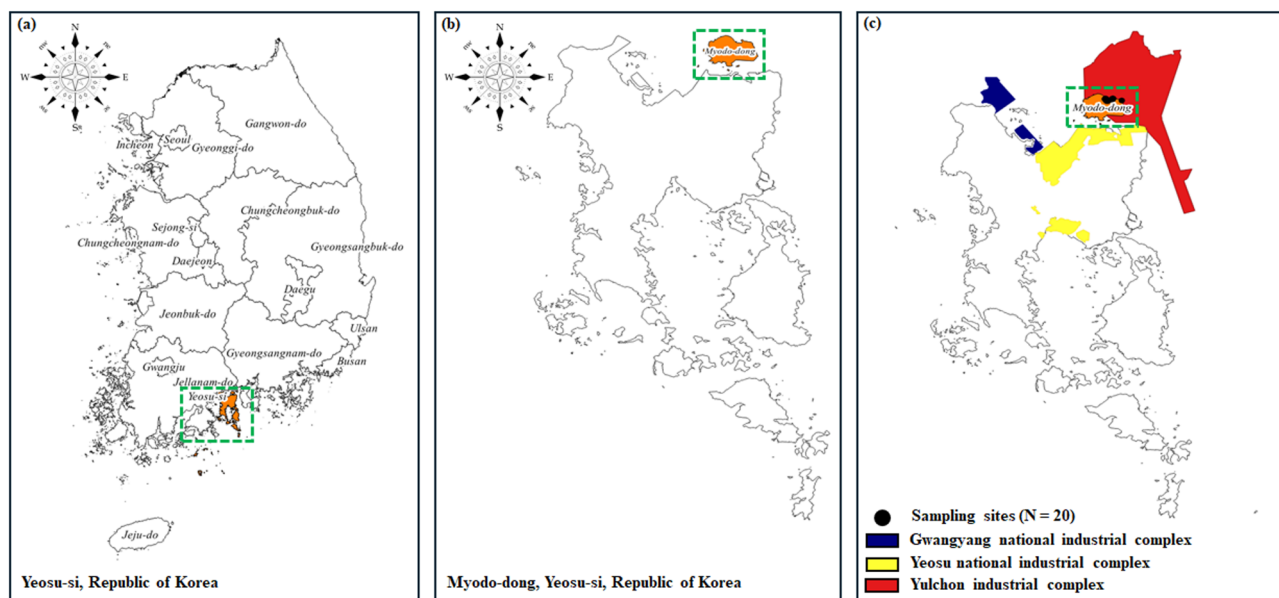


Fig. 1. Geographical location of study area. (a) Location of Yeosu-si in the Republic of Korea. (b) Location of Myodo-dong within Yeosu-si. (c) Distribution of sampling sites ($n=20$) and surrounding industrial complexes (Gwangyang, Yeosu, and Yulchon).

of the data¹⁹. Written informed consent for the collection of indoor settled dust samples was obtained from all participating households prior to sampling. Indoor settled dust samples were collected from these households over a three-day period, from June 28 to June 30, 2023. This study was conducted in accordance with standard procedures after obtaining IRB approval from Daegu Catholic University (IRB No. CUIRB-2023-0054), and all methods were carried out in accordance with the relevant guidelines and regulations.

Sampling and analysis methods

Indoor settled dust samples were collected from the main residential spaces, primarily the living room, by retrieving dust from beneath furniture such as sofas and refrigerators in accordance with the American Society for Testing Materials International (ASTM) D 7144-05a standard method²⁰. Indoor settled dust was collected using a Tygon tube (R-3603) connected to a pump (Gilian Air Plus, Sensidyne, USA) and a 3-piece cassette (SKC, 225-3-01, MCE, 0.8 µm, 37 mm). Sampling was conducted at a flow rate of 2.5 L/min for a duration of 2 min. The collected samples were sealed in clean zipper bags (LDPE: Clean Wrap, 22 cm × 25 cm, Republic of Korea), transported to the laboratory, air-dried, weighed, and stored for further analysis. The extraction of metal components, including heavy metals, was performed using an acid digestion method with a mixed solution of 1.03 M HNO₃ and 2.23 M HCl, following the standard methods for air pollution analysis¹⁹. The analysis of heavy metals in indoor settled dust was conducted using an inductively coupled plasma optical emission spectrometer (ICP-OES; ICPE-9800, SHIMADZU, Japan). The calibration curves for each heavy metal are presented in Supplementary Fig. S1, while the limits of detection (LODs) and analytical reproducibility are provided in Supplementary Table S1.

Exposure assessment

Exposure to heavy metals from indoor settled dust was assessed via inhalation, dermal contact, and ingestion routes using standardized exposure algorithms, based on methodologies established by the U.S. EPA and the National Institute for Public Health and the Environment (RIVM)^{21,22}. These algorithms consider resuspension and inhalation of indoor settled dust, dermal contact through skin adherence and absorption, and ingestion, as shown in Eqs. (1–3). In the exposure assessment, key exposure factors including body weight (64.5 ± 12.7 kg) and inhalation rate (14.6 ± 3.2 m³/day), derived from large-scale national survey data, were incorporated as probabilistic distributions (mean ± standard deviation) in the Monte Carlo simulation to capture inter-individual variability²³. Indoor settled dust metal concentrations were also modeled as distributions, and simulation results were summarized using percentiles (25th, 50th, 75th, and 95th) to characterize variability in exposure estimates. All other exposure factors were applied as fixed default values recommended by the U.S. EPA, RIVM, and National Institute Environment Research (NIER), including ingestion rate (20 mg/day), skin adherence (3.00 × 10⁻⁷ kg/cm²), surface area (4,271 cm²), particulate emission factor (1.36 × 10⁹ m³/kg), absorption factor (0.001; Pb: 0.01), exposure frequency (350 days/year), exposure duration (25 years), and averaging time (25 years for non-carcinogenic effects; 82.7 years for carcinogenic effects)^{21,22,24}. All participants were adults aged 50 years or older with long-term residence in the study area, and residential exposure scenarios were therefore applied.

$$ADD_{inh}, LADD_{inh} = \frac{C \times InhR \times EF \times ED}{PEF \times BW \times AT} \quad (1)$$

where ADD_{inh} is the inhalation average daily dose (mg/kg/day), $LADD_{inh}$ is the inhalation lifetime average daily dose (mg/kg/day), C is the concentration of heavy metal in indoor settled dust (mg/kg), $InhR$ is the inhalation rate (m³/day); EF is the exposure frequency (days), ED is the exposure duration (years), PEF is the particulate emission factor (m³/kg), BW is the body weight (kg), and AT is the averaging time (years).

$$ADD_{der}, LADD_{der} = \frac{C \times SL \times SA \times ABS \times EF \times ED}{BW \times AT} \quad (2)$$

where ADD_{der} is the dermal average daily dose (mg/kg/day), $LADD_{der}$ is the dermal lifetime average daily dose (mg/kg/day), C is the concentration of heavy metal in indoor settled dust (mg/kg), SL is the skin adherence factor (kg/cm²), SA is the surface area (cm²), ABS is the absorption factor, EF is the exposure frequency (days), ED is the exposure duration (years), BW is the body weight (kg), and AT is the averaging time (years).

$$ADD_{ing}, LADD_{ing} = \frac{C \times IngR \times EF \times ED}{BW \times AT} \quad (3)$$

where ADD_{ing} is the ingestion average daily dose (mg/kg/day), $LADD_{ing}$ is the ingestion lifetime average daily dose (mg/kg/day), C is the concentration of heavy metal in indoor settled dust (mg/kg), $IngR$ is the ingestion rate (kg/day), EF is the exposure frequency (days), ED is the exposure duration (years), BW is the body weight (kg), and AT is the averaging time (years).

Toxicity values of heavy metals in indoor settled dust

Among the heavy metals in indoor settled dust, five heavy metals (Cu, Mn, Co, Zn, and Cr) were classified as non-carcinogenic, while three heavy metals (Pb, Cd, and Ni) were categorized as carcinogenic, making a total of eight selected heavy metals. The inhalation reference dose (RfD_{inh}) in Eq. (4) and the inhalation cancer slope factor (CSF_{inh}) in Eq. (5) were derived by considering body weight (70 kg) and inhalation rate (20 m³/day), based on the reference concentration (RfC) and inhalation unit risk (IUR) values for Pb, Cd, Ni, and Mn²⁵.

$$RfD_{inh} = \frac{RfC \times 20 \text{ m}^3/\text{day}}{70 \text{ kg}} \quad (4)$$

where RfD_{inh} is the inhalation reference dose (mg/kg/day) and RfC is the reference concentration (mg/m³).

$$CSF_{inh} = \frac{IUR \times 70 \text{ kg}}{20 \text{ m}^3/\text{day}} \times 1,000 \mu \text{ g/mg} \quad (5)$$

where CSF_{inh} is the inhalation cancer slope factor (mg/kg/day)⁻¹ and IUR is inhalation unit risk (μg/m³)⁻¹.

The dermal reference dose (RfD_{der}) in Eq. (6) and the dermal cancer slope factor (CSF_{der}) in Eq. (7) were calculated by applying the gastrointestinal absorption factor (ABS_{GI}) to the ingestion reference dose (RfD_{ing}) and ingestion cancer slope factor (CSF_{ing}) of Pb, Mn, Co, Zn, and Cr²⁶. The RfD and CSF values for each exposure route of heavy metals are presented in Supplementary Table S2.

$$RfD_{der} = RfD_{ing} \times ABS_{GI} \quad (6)$$

where RfD_{der} is the dermal reference dose (mg/kg/day), RfD_{ing} is the ingestion reference dose (mg/kg/day), and ABS_{GI} is the gastrointestinal absorption factor (Pb: 1.00, Ni: 0.04).

$$CSF_{der} = \frac{CSF_{ing}}{ABS_{GI}} \quad (7)$$

where CSF_{der} is the dermal cancer slope factor (mg/kg/day)⁻¹, CSF_{ing} is the ingestion cancer slope factor (mg/kg/day)⁻¹, ABS_{GI} is the gastrointestinal absorption factor (Mn: 0.04, Co: 0.25, Cr: 0.013).

Risk assessment

The hazard quotient (HQ) for non-carcinogenic substances was obtained by calculating the ratio of the average daily dose (ADD) to the reference dose (RfD) for each exposure route (Eq. (8))²⁶. The cancer risk (CR) was calculated as the product of the lifetime average daily dose (LADD) and the cancer slope factor (CSF) for each exposure route (Eq. (9))²¹. The hazard index (HI) and total cancer risk (TCR) were calculated as the sums of HQ and CR values across all exposure routes, respectively (Eqs. (10–11))²⁷. Monte Carlo simulation was applied to incorporate variability and uncertainty, generating probabilistic distributions of HQ, HI, CR, and TCR. Simulation outputs were summarized as percentiles (25th, 50th, 75th, and 95th) together with two-sided 95% uncertainty intervals (2.5th–97.5th). Risk characterization was conducted based on the proportion of simulated outcomes in which the aggregated indices exceeded the thresholds (HI ≥ 1 for non-carcinogenic risk; TCR ≥ 1.00 × 10⁻⁶ for carcinogenic risk). In addition, sensitivity analysis was performed using partial rank correlation coefficients (PRCC) between key input parameters (metal concentration, inhalation rate, and body weight) and probabilistic risk outcomes (HI and TCR) to identify the major contributors to output variability.

$$HQ_{inh, der, ing} = \frac{ADD_{inh, der, ing}}{RfD_{inh, der, ing}} \quad (8)$$

where HQ is the hazard quotient, ADD is the average daily dose (mg/kg/day), and RfD is the reference dose (mg/kg/day).

$$CR_{inh, der, ing} = LADD_{inh, der, ing} \times CSF_{inh, der, ing} \quad (9)$$

where CR is the cancer risk, LADD is the lifetime average daily dose (mg/kg/day), and CSF is cancer slope factor (mg/kg/day)⁻¹.

$$HI = \sum HQ = HQ_{inh} + HQ_{der} + HQ_{ing} \quad (10)$$

where HI is the hazard index, HQ_{inh} is the inhalation hazard quotient, HQ_{der} is the dermal hazard quotient, and HQ_{ing} is the ingestion hazard quotient.

$$TCR = \sum CR = CR_{inh} + CR_{der} + CR_{ing} \quad (11)$$

where TCR is the total cancer risk, CR_{inh} is the inhalation cancer risk, CR_{der} is the dermal cancer risk, and CR_{ing} is the ingestion cancer risk.

Proposal of exposure limits for heavy metals in indoor settled dust

The exposure limit for non-carcinogenic heavy metals in indoor settled dust was determined by calculating the concentration at which the HI remains < 1, as shown in Eq. (12), and for carcinogenic heavy metals, by back-calculation to determine the concentration at which the TCR remains < 1.00 × 10⁻⁶, as shown in Eq. (13), using default exposure factors summarized in Supplementary Table S3.

$$C = \frac{BW \times AT}{EF \times ED \times \left(\frac{InhR}{PEF \times RfD_{inh}} + \frac{SL \times SA \times ABS}{RfD_{der}} + \frac{IngR}{RfD_{ing}} \right)} \quad (12)$$

where C is the concentration of heavy metal in indoor settled dust (mg/kg), BW is the body weight (kg), AT is the averaging time (years), EF is the exposure frequency (days), ED is the exposure duration (years), $InhR$ is the inhalation rate (m^3/day), PEF is the particulate emission factor (m^3/kg), RfD_{inh} is the inhalation reference dose (mg/kg/day), SL is the skin adherence factor (mg/cm^2), SA is the surface area (cm^2), ABS is the absorption factor, RfD_{der} is the dermal reference dose (mg/kg/day), $IngR$ is the ingestion rate (kg/day), and RfD_{ing} is the ingestion reference dose (mg/kg/day).

$$C = \frac{1.00 \times 10^{-6} \times BW \times AT}{EF \times ED \times \left(\frac{InhR \times CSF_{inh}}{PEF} + SL \times SA \times ABS \times CSF_{der} + IngR \times CSF_{ing} \right)} \quad (13)$$

where C is the concentration of heavy metal in indoor settled dust (mg/kg), BW is the body weight (kg), AT is the averaging time (years), EF is the exposure frequency (days), ED is the exposure duration (years), $InhR$ is the inhalation rate (m^3/day), CSF_{inh} is the inhalation cancer slope factor (mg/kg/day) $^{-1}$, PEF is the particulate emission factor (m^3/kg), SL is the skin adherence factor (mg/cm^2), SA is the surface area (cm^2), ABS is the absorption factor, CSF_{der} is the dermal cancer slope factor (mg/kg/day) $^{-1}$, $IngR$ is the ingestion rate (kg/day), and CSF_{ing} is the ingestion cancer slope factor (mg/kg/day) $^{-1}$.

Source tracking

Heavy metal concentrations were log-transformed to reduce skewness and approximate a normal distribution. Pearson correlation analysis was performed to assess linear relationships between metal concentrations²⁸. Normality of the log-transformed data was evaluated using the Shapiro–Wilk test. Principal component analysis (PCA) was conducted on standardized heavy metal concentration data to uncover latent structures and reduce dimensionality, as described in Eq. (14). Components with eigenvalues greater than 1 and a cumulative explained variance exceeding 80% were retained based on the Kaiser criterion²⁹. Scree plots were used to determine the optimal number of components. Each principal component represents a linear combination of the original variables that maximizes the explained variance³⁰. Component loadings were examined to interpret the grouping patterns of the heavy metals³¹.

$$PC_i = a_{i1}V_1 + a_{i2}V_2 + \dots + a_{ij}V_j \quad (14)$$

where PC_i is the i -th principal component, V_j is the j -th original observation variable, a_{ij} is the loading coefficient, representing PC_i and V_j , and n is the total number of original variables.

Subsequently, hierarchical cluster analysis (HCA) was conducted to group the samples according to the compositional patterns revealed by PCA³². Euclidean distance was used to quantify dissimilarity between samples, as defined in Eq. (15)³³. Ward's linkage method was employed to calculate inter-cluster distances while minimizing within-cluster variance, as described in Eq. (16)³⁴. The resulting dendrogram was analyzed to interpret the structural relationships among the identified sources.

$$d(x_i, x_j) = \sqrt{\sum_{k=1}^p (x_{ik} - x_{jk})^2} \quad (15)$$

where x_{ik} and x_{jk} represent the contributions of species i and j to source k , and p is the number of sources.

$$\Delta(C_i, C_j) = \frac{n_i n_j}{n_i + n_j} (\bar{x}_i - \bar{x}_j)^2 \quad (16)$$

where C_i and C_j denote the two clusters being merged, n_i and n_j are the numbers of elements in each cluster, and \bar{x}_i and \bar{x}_j are the respective cluster centroids.

Positive matrix factorization (PMF) was applied to the measured heavy metal concentration matrix to identify source profiles and estimate their contributions, subject to non-negativity constraints, as described in Eq. (17)³⁶.

$$x_{ij} = \sum_{k=1}^p g_{ik} f_{kj} + e_{ij} \quad (17)$$

where x_{ij} is the observed concentration of species j in sample i , g_{ik} is the contribution of source k to sample i , f_{kj} is the fractional concentration of species j in source k , and e_{ij} is the residual.

The PMF model is grounded in the principles of factor analysis, employing weighted least-squares minimization based on the individual uncertainties of the measured data. The model incorporates uncertainty by minimizing the objective function Q , as defined in Eq. (18), which reflects the measurement uncertainties^{35,36}. In this study, uncertainty was estimated according to the method outlined in the EPA PMF 5.0 user guide³⁷, which recommends incorporating both relative error and detection limit information. Model performance was assessed using the ratio of the observed Q value to its expected value (Q/Q_{exp}), with values close to 1 indicating that the model adequately reproduced the observed data within the bounds of analytical uncertainty. In addition, bootstrap resampling was performed with 300 iterations to evaluate the robustness of the factorization results.

For each iteration, source profiles were recalculated, and 95% confidence intervals (2.5th–97.5th percentiles) were derived, thereby quantifying the uncertainty associated with the source profiles.

$$Q = \sum_{i=1}^n \sum_{j=1}^m \left[\frac{x_{ij} - \sum_{k=1}^p g_{ik} f_{kj}}{u_{ij}} \right] \tag{18}$$

where x_{ij} is the measured concentration of species j in sample i , g_{ik} is the contribution of factor k to sample i , f_{kj} is the profile of species j in factor k , u_{ij} is the uncertainty associated with the concentrations of species j in sample i , n is the total number of samples, m is the total number of chemical species, and p is the number of factors.

In this study, a Python-based PMF model was implemented using a non-negative matrix factorization (NMF) framework. This approach incorporates key features of the EPA model, including the use of uncertainty-weighted residuals and diagnostic evaluation through comparisons between observed and expected model fit statistics, as defined in Eq. (19)³⁸.

$$X \approx WH \tag{19}$$

where X is an $M \times N$ matrix representing the concentrations of M chemical species across N samples, W is an $M \times L$ basis matrix describing source profiles, and H is an $L \times N$ coefficient matrix representing source contributions.

In addition, cosine similarity was employed to assess the compositional similarity between the PMF-resolved source profiles and industry-specific emission profiles obtained from the national the pollutant release and transfer register (PRTR), as described in Eq. (20)⁴⁰. The comparison was restricted to metals that were common to both datasets. For each PMF-resolved source, PRTR sector with the highest cosine similarity was identified to aid in source interpretation. A similarity threshold of 0.6 was applied, and only matches exceeding this value were considered compositionally meaningful⁴¹. To trace emission sources of heavy metals not listed in the PRTR, indoor dust concentrations were compared with fenceline monitoring data near an industrial complex. Regression analyses based on PMF-resolved sources identified the source with the highest coefficient of determination (R^2) as the most probable contributor.

$$\cos(\theta) = \frac{\sum_{i=1}^n A_i B_i}{\sqrt{\sum_{i=1}^n A_i^2 \times B_i^2}} \tag{20}$$

where A_i and B_i represent the contributions of metal i to the PMF-resolved source and PRTR-based profile respectively, and n is the total number of metals included in the comparison.

Results
Concentration of heavy metals in indoor settled dust

The concentrations of heavy metals in 20 indoor settled dust samples were analyzed. The statistical summary is provided in Table 1 and includes the arithmetic mean (AM), standard deviation (SD), geometric mean (GM), geometric standard deviation (GSD), minimum (Min), and maximum (Max) values. Among all metals, Zn had the highest maximum concentration at 4,912.01 µg/g, while Cd had the lowest at 0.001 µg/g. The average concentrations of heavy metals in indoor settled dust decreased in the following order: Zn > Mn > Cu > Cr > Pb > Ni > Co > Cd.

Health risk assessment of heavy metals in indoor settled dust
Exposure assessment

The probabilistic assessment of five non-carcinogenic heavy metals in indoor settled dust demonstrated that ingestion was the predominant exposure route, followed by dermal contact and inhalation (Table 2). Zn

Heavy metal	Indoor settled dust (N=20)			
	AM ± SD (µg/g)	GM (GSD) (µg/g)	Min (µg/g)	Max (µg/g)
Cu	264.38 ± 280.59	194.25 (2.05)	85.49	1,206.94
Mn	1,267.69 ± 367.84	1,218.99 (1.33)	671.49	2,100.27
Co	8.11 ± 6.35	6.01 (2.30)	1.35	24.60
Zn	1,768.34 ± 1,304.81	1,332.61 (2.23)	361.53	4,912.01
Cr	220.02 ± 181.00	159.69 (2.32)	41.82	609.67
Pb	159.92 ± 124.80	115.99 (2.39)	26.98	438.01
Cd	3.73 ± 7.47	0.08 (41.48)	0.001	28.33
Ni	67.45 ± 42.03	56.97 (1.81)	16.85	169.08

Table 1. Concentration of heavy metals in indoor settled dust. AM: arithmetic mean; SD: standard deviation; GM: geometric mean; GSD: geometric standard deviation; Min: minimum; Max: maximum.

Heavy metal	Exposure route	ADD percentiles			
		25th	50th	75th	95th
Cu	Inhalation	1.55×10^{-8}	2.89×10^{-8}	5.37×10^{-8}	1.31×10^{-7}
	Dermal	1.93×10^{-6}	3.53×10^{-6}	6.44×10^{-6}	1.54×10^{-5}
	Ingestion	3.01×10^{-5}	5.50×10^{-5}	1.01×10^{-4}	2.40×10^{-4}
Mn	Inhalation	1.46×10^{-7}	1.94×10^{-7}	2.57×10^{-7}	3.85×10^{-7}
	Dermal	1.86×10^{-5}	2.35×10^{-5}	2.98×10^{-5}	4.27×10^{-5}
	Ingestion	2.91×10^{-4}	3.67×10^{-4}	4.66×10^{-4}	6.67×10^{-4}
Co	Inhalation	6.09×10^{-10}	1.02×10^{-9}	1.69×10^{-9}	3.53×10^{-9}
	Dermal	7.62×10^{-8}	1.24×10^{-7}	2.02×10^{-7}	4.09×10^{-7}
	Ingestion	1.19×10^{-6}	1.94×10^{-6}	3.15×10^{-6}	6.39×10^{-6}
Zn	Inhalation	1.38×10^{-7}	2.26×10^{-7}	3.69×10^{-7}	7.49×10^{-7}
	Dermal	1.73×10^{-5}	2.76×10^{-5}	4.40×10^{-5}	8.66×10^{-5}
	Ingestion	2.71×10^{-4}	4.31×10^{-4}	6.88×10^{-4}	1.35×10^{-3}
Cr	Inhalation	1.59×10^{-8}	2.70×10^{-8}	4.57×10^{-8}	9.77×10^{-8}
	Dermal	1.99×10^{-6}	3.29×10^{-6}	5.46×10^{-6}	1.14×10^{-5}
	Ingestion	3.11×10^{-5}	5.14×10^{-5}	8.52×10^{-5}	1.77×10^{-4}

Table 2. ADD percentiles (25th–95th) of heavy metals by exposure route. ADD: average daily dose.

Heavy metal	Exposure route	LADD percentiles			
		25th	50th	75th	95th
Pb	Inhalation	3.64×10^{-9}	6.05×10^{-9}	1.01×10^{-8}	2.10×10^{-8}
	Dermal	4.55×10^{-6}	7.40×10^{-6}	1.20×10^{-5}	2.43×10^{-5}
	Ingestion	7.11×10^{-6}	1.15×10^{-5}	1.88×10^{-5}	3.80×10^{-5}
Cd	Inhalation	3.31×10^{-11}	7.99×10^{-11}	1.93×10^{-10}	6.84×10^{-10}
	Dermal	4.11×10^{-9}	9.79×10^{-9}	2.33×10^{-8}	8.11×10^{-8}
	Ingestion	6.42×10^{-8}	1.53×10^{-7}	3.63×10^{-7}	1.27×10^{-6}
Ni	Inhalation	1.77×10^{-9}	2.75×10^{-9}	4.27×10^{-9}	8.01×10^{-9}
	Dermal	2.23×10^{-7}	3.36×10^{-7}	5.07×10^{-7}	9.20×10^{-7}
	Ingestion	3.48×10^{-6}	5.24×10^{-6}	7.91×10^{-6}	1.44×10^{-5}

Table 3. LADD percentiles (25th–95th) of heavy metals by exposure route. LADD: lifetime average daily dose.

Heavy metal	HQ _{inh} (25th–95th)	HQ _{der} (25th–95th)	HQ _{ing} (25th–95th)	HI (25th–95th)	Risk exceedance (%)
Cu	3.84×10^{-7} – 3.27×10^{-6}	1.61×10^{-4} – 1.28×10^{-3}	7.53×10^{-4} – 6.00×10^{-3}	9.15×10^{-4} – 7.29×10^{-3}	0.00
Mn	1.02×10^{-2} – 2.69×10^{-2}	3.33×10^{-3} – 7.63×10^{-3}	2.08×10^{-3} – 4.76×10^{-3}	1.58×10^{-2} – 3.88×10^{-2}	0.00
Co	1.07×10^{-4} – 6.18×10^{-4}	1.52×10^{-5} – 8.18×10^{-5}	3.97×10^{-3} – 2.13×10^{-2}	4.09×10^{-3} – 2.20×10^{-2}	0.00
Zn	1.84×10^{-6} – 9.99×10^{-6}	2.31×10^{-3} – 1.16×10^{-2}	9.02×10^{-4} – 4.51×10^{-3}	3.22×10^{-3} – 1.61×10^{-2}	0.00
Cr	8.16×10^{-7} – 5.01×10^{-6}	1.02×10^{-4} – 5.82×10^{-4}	2.07×10^{-5} – 1.18×10^{-4}	1.24×10^{-4} – 7.05×10^{-4}	0.00

Table 4. HQ and HI percentiles (25th–95th) of heavy metals and corresponding risk exceedance. HQ_{inh}: inhalation hazard quotient; HQ_{der}: dermal hazard quotient; HQ_{ing}: ingestion hazard quotient; HI: hazard index.

consistently showed the highest exposure across all routes, with median ADD_{ing}, ADD_{der}, and ADD_{inh} values of 4.31×10^{-4} , 2.76×10^{-5} , and 2.26×10^{-7} mg/kg/day, respectively. In contrast, Co exhibited the lowest exposures, with values of 1.94×10^{-6} mg/kg/day for ingestion, 1.24×10^{-7} mg/kg/day for dermal contact, and 1.02×10^{-9} mg/kg/day for inhalation. The three carcinogenic heavy metals showed the same trend as the ADD results, with ingestion as the dominant exposure route, followed by dermal contact and inhalation (Table 3). Pb presented the highest exposures, with median LADD_{ing}, LADD_{der}, and LADD_{inh} values of 1.15×10^{-5} , 7.40×10^{-6} , and 6.05×10^{-9} mg/kg/day. Conversely, Cd showed the lowest exposures, with ingestion, dermal, and inhalation values of 1.53×10^{-7} , 9.79×10^{-9} , and 7.99×10^{-11} mg/kg/day.

Risk assessment

The probabilistic risk assessment showed that HQ and HI values of non-carcinogenic metals in indoor settled dust remained below 1 across the 25th–95th percentile range (Table 4). Mn recorded the highest HQ_{inh}, ranging

Heavy metal	CR _{inh} (25th–95th)	CR _{der} (25th–95th)	CR _{ing} (25th–95th)	TCR (25th–95th)	Risk exceedance (%)
Pb	1.53×10^{-10} – 8.83×10^{-10}	3.87×10^{-8} – 2.07×10^{-7}	6.04×10^{-8} – 3.23×10^{-7}	9.93×10^{-8} – 5.31×10^{-7}	0.59
Cd	2.08×10^{-10} – 4.31×10^{-9}	2.51×10^{-8} – 4.95×10^{-7}	3.92×10^{-7} – 7.72×10^{-6}	4.17×10^{-7} – 8.22×10^{-6}	49.75
Ni	1.49×10^{-9} – 6.73×10^{-9}	9.47×10^{-6} – 3.91×10^{-5}	5.91×10^{-6} – 2.44×10^{-5}	1.54×10^{-5} – 6.35×10^{-5}	100.00

Table 5. CR and TCR percentiles (25th–95th) of heavy metals and corresponding risk exceedance. CR_{inh}: inhalation cancer risk; CR_{der}: dermal cancer risk; CR_{ing}: ingestion cancer risk; TCR: total cancer risk.

Heavy metal		Calculated concentration (µg/g)	Exposure limit (µg/g)
Non-carcinogenic	Cu	110,806.6	110,805.0
	Mn	59,930.0	59,925.0
	Co	977.6	975.0
	Zn	801,778.9	801,775.0
	Cr	845,118.3	845,115.0
Carcinogenic	Pb	796.5	795.0
	Cd	1.7	1.5
	Ni	2.5	2.0

Table 6. Exposure limits of heavy metals in indoor settled dust.

from 1.02×10^{-2} to 2.69×10^{-2} , while Zn showed the highest HQ_{der}, ranging from 2.31×10^{-3} to 1.16×10^{-2} , and Co exhibited the highest HQ_{ing}, ranging from 3.97×10^{-3} to 2.13×10^{-2} . The HI, which represents the combined non-carcinogenic risks from all exposure routes, also remained below 1. The risk exceedance percentage for HI was 0%, confirming the absence of non-carcinogenic health risks. The probabilistic risk assessment further showed that CR and TCR values of carcinogenic metals in indoor settled dust were distributed across the 25th–95th percentiles, with exceedances of the acceptable threshold of 1.00×10^{-6} observed for Cd and Ni but not for Pb (Table 5). Pb presented no potential health risks across individual exposure routes. In contrast, Cd exceeded the acceptable threshold CR_{ing} ranging from 3.92×10^{-7} to 7.72×10^{-6} , indicating that ingestion was the dominant contributor. Ni posed the greatest concern, with CR_{der} ranging from 9.47×10^{-6} to 3.91×10^{-5} and CR_{ing} ranging from 5.91×10^{-6} to 2.44×10^{-5} , both well above the threshold. The TCR ranged from 9.93×10^{-8} to 5.31×10^{-7} for Pb, consistently below the acceptable threshold of 1.00×10^{-6} , although a negligible exceedance of 0.59% was observed in the simulation. In contrast, TCR values ranged from 4.17×10^{-7} to 8.22×10^{-6} for Cd (49.75% exceedance) and from 1.54×10^{-5} to 6.35×10^{-5} for Ni (100% exceedance). The probabilistic distributions of HI and TCR derived from Monte Carlo simulations are illustrated in Supplementary Fig. S2. The sensitivity analysis based on PRCC identified concentration as the strongest positive contributor to both HI and TCR (PRCC: +0.95 to +1.00), while body weight showed a strong negative influence (PRCC: −0.89 to −0.91). Inhalation rate generally had only a minor effect (PRCC: 0.00 to +0.06), except for Mn where a positive contribution was observed (PRCC: +0.83), as illustrated in Supplementary Fig. S3.

Proposal of exposure limits for heavy metals in indoor settled dust

A back-calculation approach was used to determine exposure limits for non-carcinogenic and carcinogenic heavy metals in indoor settled dust, based on the HI and TCR, respectively, with target values of HI < 1 for non-carcinogens and TCR < 1.00×10^{-6} for carcinogens, with results summarized in Table 6. Among the non-carcinogenic metals assessed, Cr had the highest allowable concentration at 845,118.3 µg/g, followed by Zn, Cu, Mn, and Co, with values of 801,778.9, 110,806.6, 59,930.0, and 977.6 µg/g, respectively. Based on these estimates, corresponding exposure limits are proposed to protect human health. The proposed values are approximately 845,115.0, 801,775.0, 110,805.0, 59,925.0, and 975.0 µg/g for Cr, Zn, Cu, Mn, and Co, respectively. For carcinogenic heavy metals (Pb, Ni, and Cd), the allowable concentrations calculated for adults based on this approach were 796.5 µg/g for Pb, 1.7 µg/g for Cd, and 2.5 µg/g for Ni. Accordingly, the proposed exposure limits were set at 795.0 µg/g for Pb, 1.5 µg/g for Cd, and 2.0 µg/g for Ni.

Source tracking

Pearson correlation analysis

The Shapiro–Wilk test confirmed that log transformation improved normality, thereby supporting the validity of applying Pearson correlation analysis, which revealed significant relationships among heavy metal concentrations in indoor settled dust (Fig. 2). Strong positive correlations were observed between Mn, Co, Zn, Cr, and Pb including Cr–Pb ($r=0.987$), Mn–Zn ($r=0.977$), Co–Cr ($r=0.940$), Co–Pb ($r=0.928$), Zn–Cr ($r=0.760$), Mn–Cr ($r=0.755$), Zn–Pb ($r=0.735$), and Mn–Pb ($r=0.727$). Moderate positive correlations were also observed for Mn–Co ($r=0.694$), Co–Zn ($r=0.688$), Cu–Zn ($r=0.647$), Cu–Ni ($r=0.599$), and Cu–Mn ($r=0.596$). All correlations were statistically significant ($p<0.01$). In contrast, Cd appeared to behave independently from the other heavy metals, as it showed no statistically significant positive correlations and exhibited weak to negative associations with most of them.

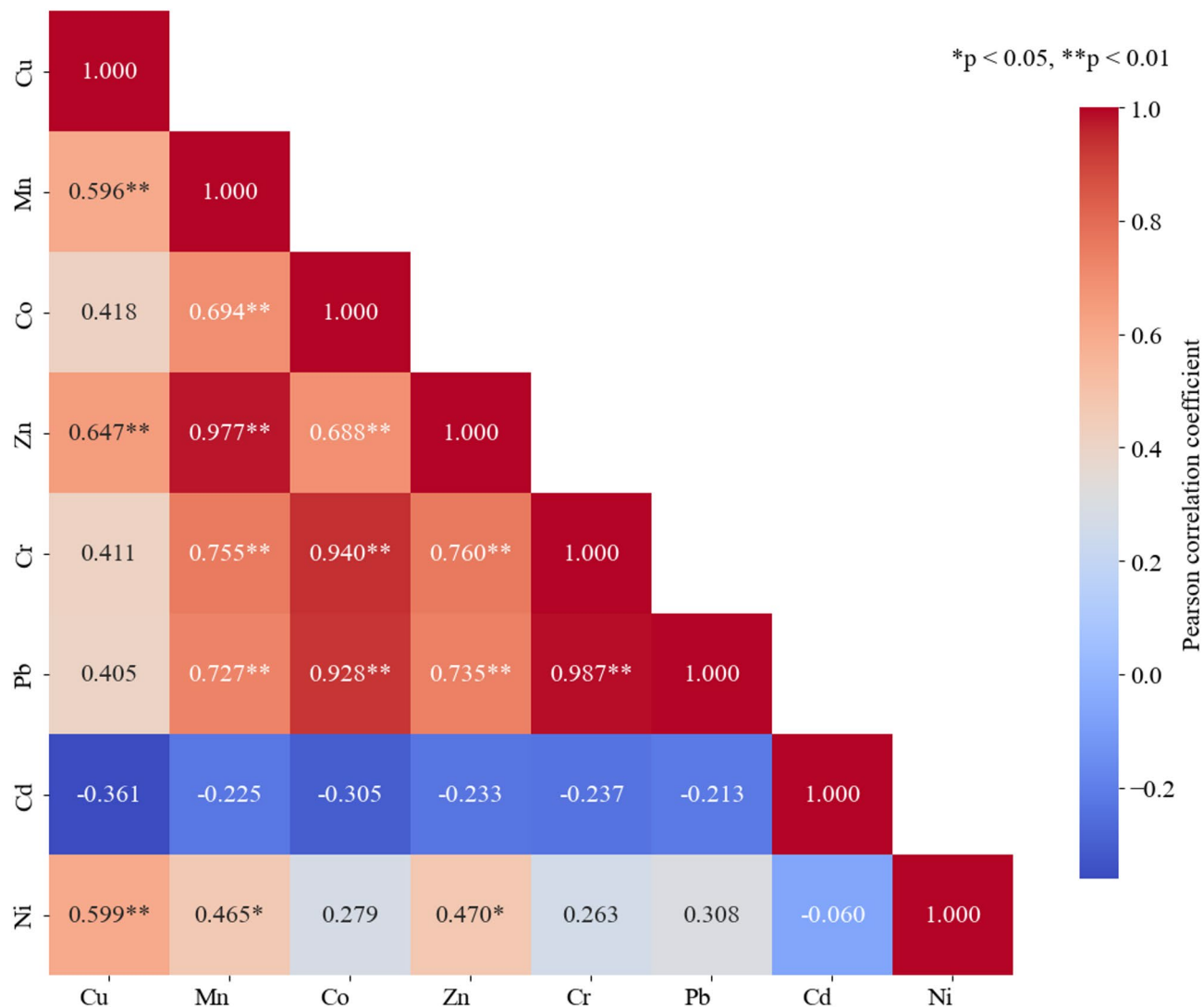


Fig. 2. Pearson correlation analysis of heavy metal concentrations in indoor settled dust.

Principal component analysis

The PCA results extracted three principal components (PC1, PC2, and PC3) with eigenvalues greater than 1, which together explained 89.862% of the total variance (Fig. 3). PC1 was primarily associated with Mn (loading=0.425), Co (loading=0.395), Zn (loading=0.420), Cr (loading=0.422), and Pb (loading=0.429), accounting for 58.143% of the total variance. PC2 was characterized by Cu (loading=0.667), and Ni (loading=0.446) explaining 18.674% of the variance. PC3 was dominated by Cd (loading=0.932), accounting for 13.025% of the variance (Table 7).

Hierarchical cluster analysis

The HCA was performed to assess compositional similarities among the eight heavy metals. As illustrated in Fig. 4, the heavy metals were categorized into three distinct clusters based on their pairwise dissimilarities. The first cluster included Mn, Co, Zn, Cr, and Pb, indicating a relatively high similarity in their compositional profiles. The second cluster comprised Cu and Ni which exhibited close interrelationships. Cd was grouped separately into a third independent cluster, reflecting a markedly different compositional pattern from the other metals. Clustering was conducted using Ward's linkage method with Euclidean distance as the dissimilarity metric, facilitating the formation of compact and statistically meaningful clusters. The resulting dendrogram clearly delineated the three groups, visually representing the underlying compositional structure of the metals. These clustering outcomes were largely consistent with the patterns identified through PCA, further supporting the multivariate relationships among the examined elements.

Positive matrix factorization

Five components were identified as the most appropriate solution for the dataset, as they provided the best model fit. As shown in Fig. 5, the Q/Q_{exp} ratio was reduced to 0.011, and the cumulative explained variance

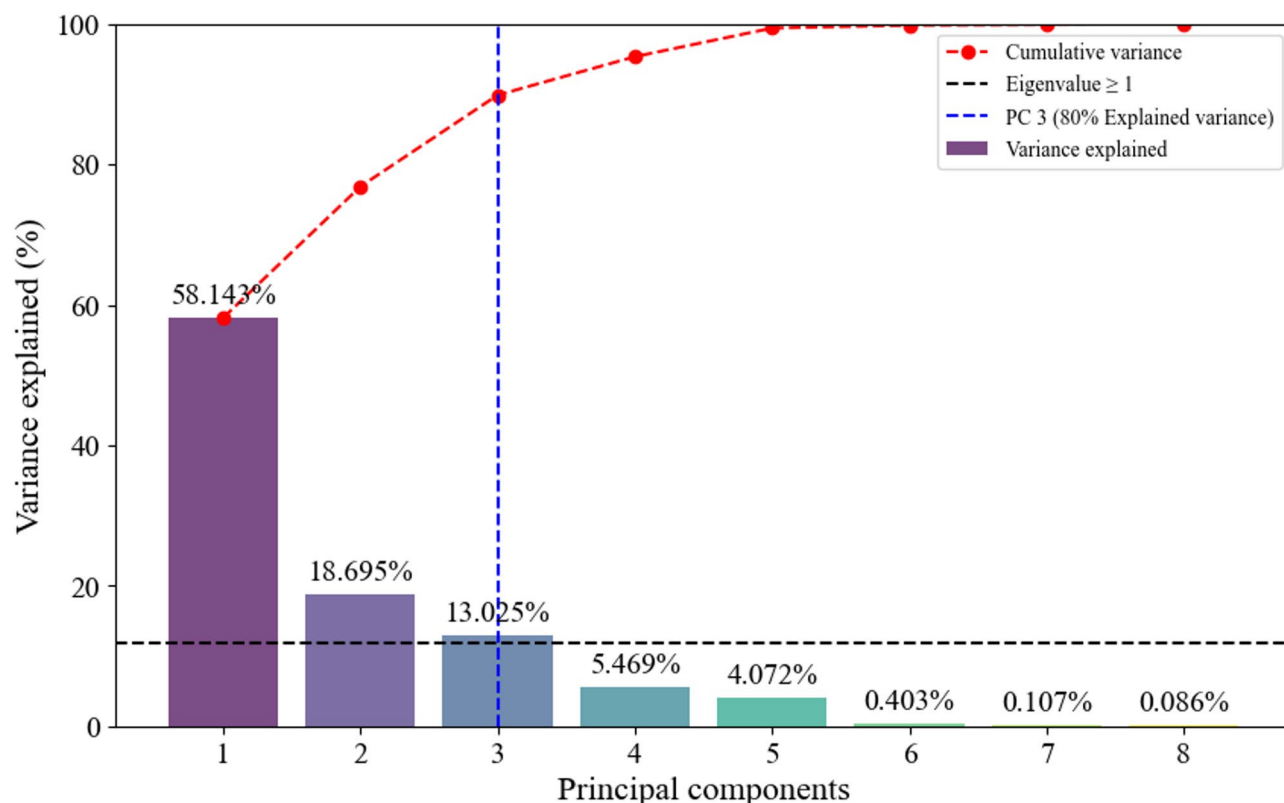


Fig. 3. Variance explained by principal components in PCA.

Component	Initial eigenvalues			Heavy metals	Component matrix		
	Total	Variance %	Cumulative %		PC1	PC2	PC3
1	4.896	58.143	58.143	Cu	0.190	0.667	-0.054
2	1.574	18.694	76.837	Mn	0.425	0.115	0.041
3	1.097	13.025	89.862	Co	0.395	-0.334	-0.196
4	0.461	5.469	95.331	Zn	0.420	0.149	0.180
5	0.343	4.072	99.403	Cr	0.422	-0.312	-0.057
6	0.034	0.403	99.806	Pb	0.429	-0.271	0.006
7	0.009	0.107	99.913	Cd	-0.055	-0.193	0.932
8	0.007	0.087	100.000	Ni	0.293	0.446	0.230
				Eigenvalues	4.896	1.574	1.097
				Total variance %	58.143	18.694	13.025
				Cumulative %	58.143	76.837	89.862

Table 7. PCA of heavy metals in indoor settled dust.

reached 98.556%, indicating that the five-component solution effectively captured the underlying structure without overfitting (Supplementary Table S4). The five source factors resolved by PMF and their heavy metal compositions are shown in Supplementary Fig. S4, while the detailed contribution profiles are summarized in Table 8. Source 1 primarily consisted of Cd, which represented 78.13% of the total Cd concentration, with only minor contributions from other heavy metals. Source 2 was mainly composed of Co (35.01%) and Mn (33.11%), whereas Cu, Cd, and Ni were not detected. Source 3 had major contributions from Zn (25.30%), and source 4 was the primary contributor to both Cu (9.45%) and Ni (47.65%). Source 5 was distinctively characterized by high contributions of Pb (28.76%) and Cr (26.16%). Bootstrap resampling with 300 iterations provided 95% confidence intervals for the heavy metal contributions, thereby allowing evaluation of the robustness of the resolved source profiles (Supplementary Fig. S5). The bootstrap results indicated that Cd exhibited the highest contribution with a median of 50.5% (95% CI: 3.5–85.5%), while Cu showed the lowest contribution with a median of 0.56% (95% CI: <0.01–14.5%). The PRTR-based sectoral emission profiles that can be compared with the PMF-derived source contribution profiles are presented in Supplementary Table S5. Source 1 was excluded from the similarity analysis because its dominant component, Cd (78.13%), was not included in the

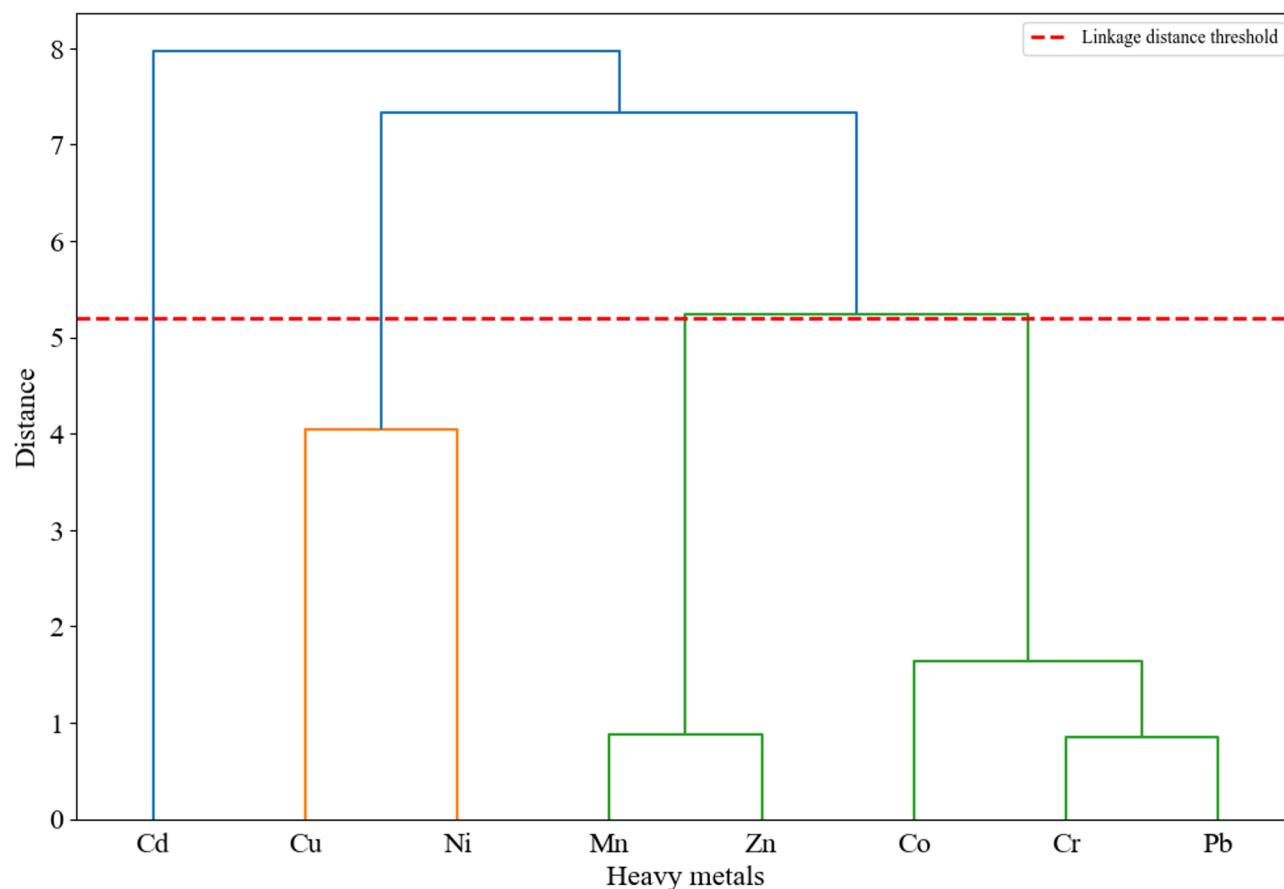


Fig. 4. Hierarchical clustering of heavy metals.

PRTR dataset. Emission sources were identified by calculating the cosine similarity based on the heavy metal compositional profiles derived from each PMF source and those of industrial sectors (Table 9). Source 2 showed the highest similarity to the manufacture of primary cells, batteries, and accumulators sector (0.921). Source 3 was closely matched with the manufacture of synthetic rubber and plastics in primary forms (0.898), while source 4 corresponded to the manufacture of basic precious and non-ferrous metals (0.862). Source 5 showed a moderate level of similarity to the manufacture of ceramic ware sector (0.686). All sources exceeded the similarity threshold of 0.6, indicating reliable compositional agreement with the corresponding PRTR sectors.

Fence monitoring

Linear regression analysis was performed to evaluate the relationship between fenceline metal concentrations and indoor settled dust levels, using monitoring data collected near a basic iron and steel manufacturing facility (Supplementary Table S6). The analysis revealed a strong positive correlation between the two datasets ($R^2 = 0.983$, $p < 0.01$), indicating that ambient emissions were clearly reflected in indoor metal concentrations (Fig. 6). Among the analyzed metals, Cd exhibited particularly consistent concentration patterns in both the fenceline and indoor environments. This result is closely associated with the interpretation of source 1 identified by PMF, which was characterized by a dominant contribution of Cd.

Discussion

This study conducted a comprehensive assessment of human exposure and health risks associated with eight heavy metals (Cu, Mn, Co, Zn, Pb, Cd, Ni, and Cr) based on indoor settled dust collected from 20 households in Myodo-dong, Yeosu, the Republic of Korea. The concentrations of heavy metals in indoor dust were used to estimate both non-carcinogenic and carcinogenic risks, and exposure limits protective of human health were proposed. In addition, multivariate statistical analyses such as Pearson correlation, PCA, and HCA were conducted to explore interrelationships among the heavy metals and identify potential patterns. Furthermore, source apportionment was performed using PMF, and for substances not included in the PRTR database, potential emission sources were identified and validated through comparative analysis with fenceline monitoring data.

An analysis of heavy metal concentrations in indoor settled dust collected from 20 households in Myodo-dong, Yeosu, revealed that the average concentration was highest for Zn, with a mean value of $1,768.34 \pm 1,304.81$ $\mu\text{g/g}$. According to a study by Roy et al. (2024)⁴², elevated concentrations of Zn in indoor settled dust have been associated with various industrial activities. The high Zn concentrations detected in Myodo-dong are likely due

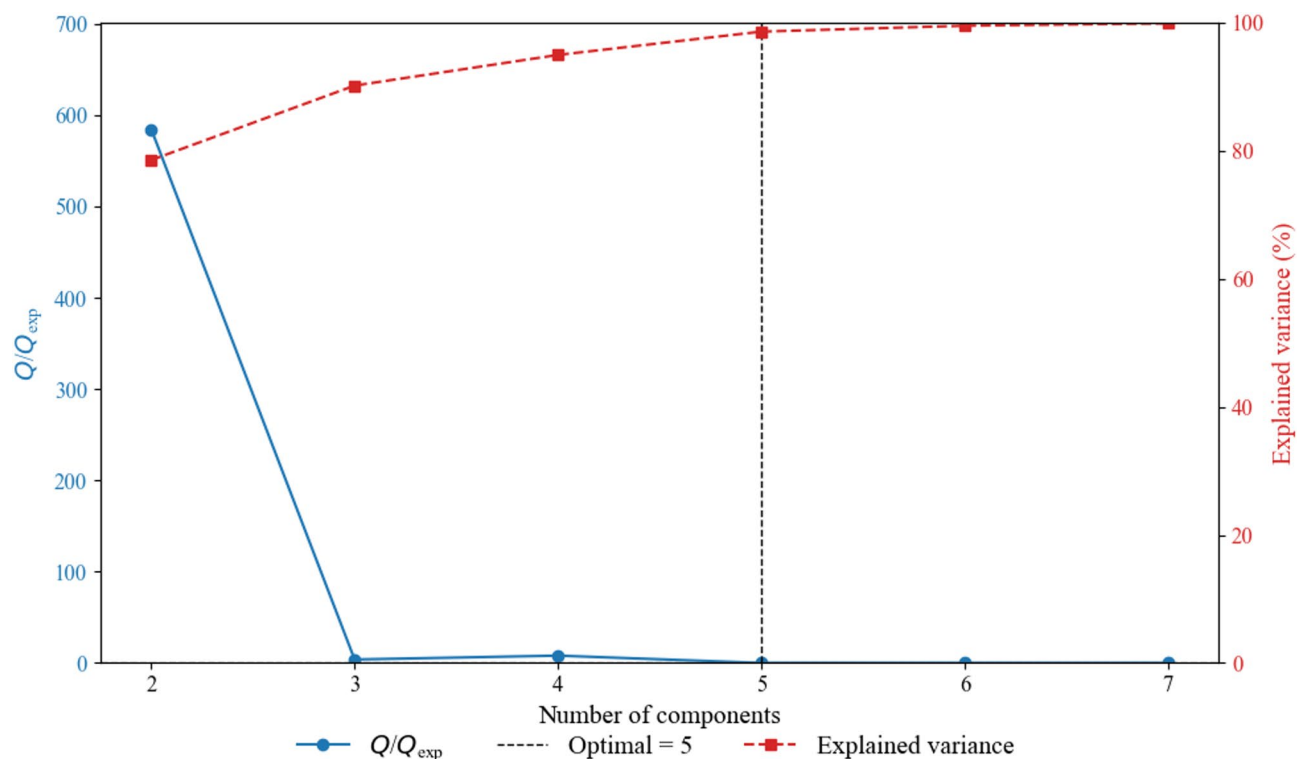


Fig. 5. Optimal PMF components based on Q/Q_{exp} and variance.

Source	Source contribution (%)							
	Cu	Mn	Co	Zn	Cr	Pb	Cd	Ni
Source 1	0.53	7.46	0.01	0.00	0.45	0.71	78.13	12.71
Source 2	0.00	33.11	35.01	3.55	19.86	8.47	0.00	0.00
Source 3	4.03	7.88	12.75	25.30	21.47	28.51	0.00	0.04
Source 4	9.45	26.77	4.41	7.66	1.54	2.53	0.00	47.65
Source 5	5.40	7.04	25.18	7.46	26.16	28.76	0.00	0.00

Table 8. Source contribution of heavy metals by the PMF model.

PMF source	Closet PRTR sector	Cosine similarity
Source 2	Manufacture of primary cells and batteries and accumulators	0.921
Source 3	Manufacture of synthetic rubber and of plastics in primary forms	0.898
Source 4	Manufacture of basic precious and non-ferrous metals	0.862
Source 5	Manufacture of ceramic ware	0.686

Table 9. Matched PRTR sectors for each PMF source based on cosine similarity metrics. Source 1 was excluded from the PRTR sector matching due to the absence of Cd, a key contributing element, in the PRTR data.

to emissions from large-scale industrial complexes such as Gwangyang National, Yeosu, and Yulchon. ADD and LADD for five non-carcinogenic and three carcinogenic metals were estimated using exposure algorithms, with dust ingestion identified as the route contributing the highest values. Consistent with the findings of Ali et al. (2018)⁴³, ingestion was identified as the most significant route for dust-related exposure. Although non-carcinogenic metals posed no significant risks, the TCR for Cd and Ni exceeded 1×10^{-6} , with Ni showing the highest concern, highlighting the need for continued monitoring. Exposure limits for five non-carcinogenic and three carcinogenic heavy metals in indoor settled dust were established through back-calculations based on HI and TCR. The relatively higher thresholds for Cr and Zn indicate their lower toxicological potency and greater tolerable exposure levels⁴⁴. In contrast, carcinogenic substances tend to have lower thresholds due to

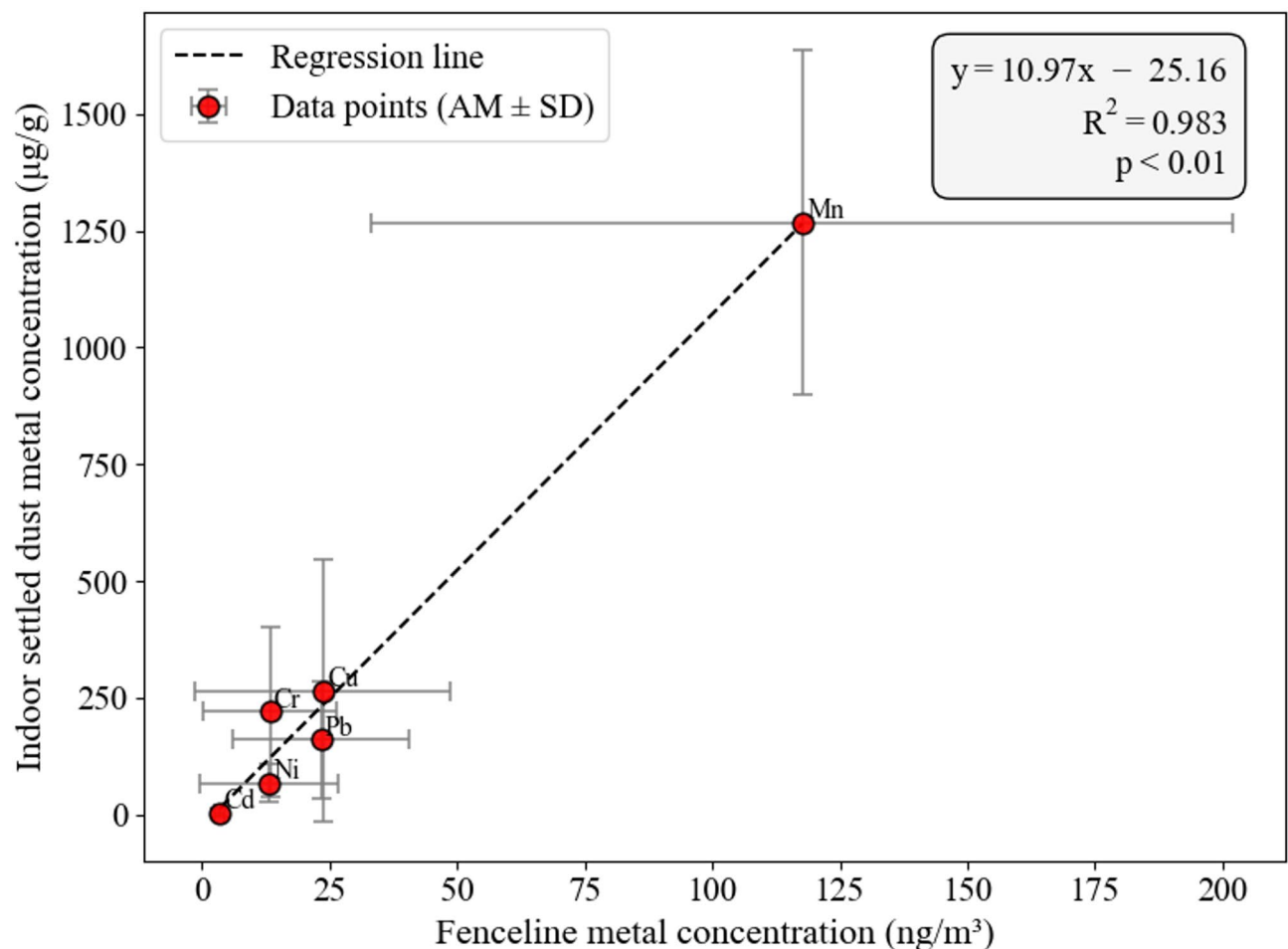


Fig. 6. Regression analysis between fenceline and indoor settled dust heavy metal concentrations.

their potential to cause adverse health effects even at low doses⁴⁵. When both the RfD and CSF are available, CSF-based values are generally preferred to better protect vulnerable populations, including children, pregnant women, and the elderly.

Pearson correlation analysis revealed strong positive correlations were observed between Mn, Co, Zn, Cr, and Pb including Cr-Pb ($r = 0.987$), Mn-Zn ($r = 0.977$), Co-Cr ($r = 0.940$), Co-Pb ($r = 0.928$) suggesting a shared emission source. The simultaneous detection of Mn, Co, Zn, Cr, and Pb may be attributed to shared industrial sources, such as the use of metal-containing materials, high-temperature processing, and recycling activities, as supported by previous studies on heavy metal emissions^{46–48}. Both PCA and HCA results showed co-occurrence of Cu and Ni, suggesting a potential link to the manufacture of basic precious and other non-ferrous metals, such as copper smelting, nickel refining, and alloy production processes that commonly emit these metals⁴⁹. The PMF analysis resolved five distinct source profiles characterized by unique elemental compositions, and bootstrap resampling with 300 iterations confirmed their robustness despite the small sample size. Comparison with sector-specific emission data from the PRTR revealed strong compositional consistency across all identified sources, with cosine similarity values exceeding 0.6⁴². Enriched in Co and Mn, source 2 showed the highest similarity with the manufacture of primary cells, batteries, and accumulators. This finding, in line with the results reported by Brown et al. (2024)⁵⁰, suggests that battery-related industrial activities may serve as a major contributor to indoor metal contamination, especially in regions close to electronic or energy materials production facilities. Source 3, enriched in Zn, was identified as being associated with the manufacture of synthetic rubber and primary-form plastics, where zinc-based compounds are commonly used as stabilizers and processing aids, potentially leading to Zn emissions during production and recycling⁵¹. The source dominated by Cu and Ni showed consistency with the results of correlation analysis, PCA, and HCA, and was identified as source 4, which was associated with the manufacture of basic precious and non-ferrous metals. This attribution is further supported by previous studies, including life cycle assessments and emission analyses, which have demonstrated that copper and nickel are major pollutants released during smelting and refining processes in the non-ferrous metal industry^{52,53}. Source 5, identified as being associated with the manufacture of ceramic ware, was characterized by elevated levels of Pb and Cr, which are commonly used in ceramic glazes and colorants and may be emitted during high-temperature firing processes^{54,55}. Cd was not included in the PRTR inventory, making it difficult to assign Source 1, which showed a predominant contribution of Cd, to a specific sector.

Nevertheless, a strong correlation between Cd concentrations at the fenceline and those found in indoor settled dust ($R^2 = 0.983$; $p < 0.01$) suggests that ambient emissions are substantially reflected indoors. This finding underscores the importance of fenceline monitoring as a complementary method for detecting emission sources that may be missing or underrepresented in inventory-based analyses, and it partly addresses the limitation of direct source attribution for Cd by providing indirect validation of its origin.

This study integrated exposure and health risk evaluation based on indoor settled dust, multivariate statistical analyses, PMF receptor modeling, and validation with PRTR and fenceline monitoring data, providing a comprehensive framework for robust source tracking even for substances not listed in emission inventories. However, several limitations remain. Although 20 out of approximately 50 households in the study area participated, which represents a relatively high sampling proportion, the overall sample size is still limited. In addition, the absence of Cd data in the PRTR inventory restricted direct source attribution. Furthermore, household-specific factors such as ventilation conditions, occupant behavior, and cleaning frequency were not considered, even though they can influence dust accumulation and human exposure levels. Future studies should apply site-specific indoor air measurements to refine inhalation exposure estimates, as this study relied on a default PEF recommended by EPA and RIVM that, while ensuring consistency and comparability with previous research, is inherently site-specific and may vary depending on meteorological conditions and indoor activities. As with all PMF applications, rotational ambiguity cannot be fully excluded. In this study, bootstrap resampling with 300 iterations provided confidence intervals that supported factor stability, partly addressing this limitation. Nonetheless, additional validation is warranted, as cosine similarity between PMF-derived profiles and PRTR sectors does not resolve alternative rotations. Future research should therefore complement this approach with displacement analysis or independent tracer validation to further strengthen source attribution.

Conclusions

This study evaluated the health risks, proposed exposure limits, and identified sources of eight heavy metals (Cu, Mn, Co, Zn, Cr, Pb, Cd, Ni) in indoor settled dust from households in Myodo-dong, an industrially impacted area in the Republic of Korea. Zn was the most abundant, and ingestion was the main exposure route. While non-carcinogenic risks were within safe limits, carcinogenic risks for Ni and Cd exceeded acceptable thresholds. Source tracking were first identified through multivariate analyses (correlation analysis, PCA, HCA), and five emission sources were then quantitatively resolved using PMF. These sources were validated against PRTR sector profiles using cosine similarity. Cd, although not included in the PRTR inventory, was a dominant PMF source and showed a strong correlation with fenceline data. The findings highlight the need for integrated monitoring and modeling to capture sources overlooked by current inventories.

Data availability

The data and material used in this study are available from the corresponding author on request.

Received: 22 August 2025; Accepted: 6 October 2025

Published online: 12 November 2025

References

- Chen, R., Tu, H. & Chen, T. Potential application of living microorganisms in the detoxification of heavy metals. *Foods* **11** (13), 1905. <https://doi.org/10.3390/foods11131905> (2022).
- Adnan, M., Xiao, B., Xiao, P., Zhao, P. & Bibi, S. Heavy metal, waste, COVID-19, and rapid industrialization in this modern era—Fit for sustainable future. *Sustainability* **14** (8), 4746. <https://doi.org/10.3390/su14084746> (2022).
- Saxena, V. Water quality, air pollution, and climate change: investigating the environmental impacts of industrialization and urbanization. *Water Air Soil Pollut.* **236** (2), 73. <https://doi.org/10.1007/s11270-024-07702-4> (2025).
- Baek, K. M., Kim, M. J., Kim, J. Y., Seo, Y. K. & Baek, S. O. Characterization and health impact assessment of hazardous air pollutants in residential areas near a large iron-steel industrial complex in Korea. *Atmos. Pollut. Res.* **11** (10), 1754–1766. <https://doi.org/10.1016/j.apr.2020.07.009> (2020).
- Jomova, K., Alomar, S. Y., Nepovimova, E., Kuca, K. & Valko, M. Heavy metals: Toxicity and human health effects. *Arch. Toxicol.* **1–57**. <https://doi.org/10.1007/s00204-024-03903-2> (2024).
- Parui, R. et al. Impact of heavy metals on human health. In *Remediation of Heavy Metals: Sustainable Technologies and Recent Advances*. 47–81. (2024). <https://doi.org/10.1002/9781119853589.ch4>
- Sulaiman, F. R., Bakri, N. I. F., Nazmi, N. & Latif, M. T. Assessment of heavy metals in indoor dust of a university in a tropical environment. *Environ. Forensics*. **18** (1), 74–82. <https://doi.org/10.1080/15275922.2016.1263903> (2017).
- Zheng, K. et al. Current status of indoor dust PBDE pollution and its physical burden and health effects on children. *Environ. Sci. Pollut. Res.* **30** (8), 19642–19661. <https://doi.org/10.1007/s11356-022-24723-w> (2023).
- Barrio-Parra, F., De Miguel, E., Lázaro-Navas, S., Gómez, A. & Izquierdo, M. Indoor dust metal loadings: a human health risk assessment. *Expo Health*. **10** (1), 41–50. <https://doi.org/10.1007/s12403-017-0244-z> (2018).
- Somsunun, K. et al. Health risk assessment of heavy metals in indoor household dust in urban and rural areas of Chiang Mai and Lamphun provinces. *Thail. Toxics*. **11** (12), 1018. <https://doi.org/10.3390/toxics11121018> (2023).
- Rahman, M. S. et al. Assessing risk to human health for heavy metal contamination through street dust in the Southeast Asian megacity: Dhaka, Bangladesh. *Sci. Total Environ.* **660**, 1610–1622. <https://doi.org/10.1016/j.scitotenv.2018.12.425> (2019).
- Sajedi Sabegh, S., Mansouri, N., Taghavi, L. & Mirzahosseini, S. A. Pollution status, origin, and health risk assessment of toxic metals in deposited indoor and outdoor urban dust. *Int. J. Environ. Sci. Technol.* **20** (3), 2471–2486. <https://doi.org/10.1007/s1376-022-04530-z> (2023).
- Huang, M. et al. Contamination and risk assessment (based on bioaccessibility via ingestion and inhalation) of metal (loid) s in outdoor and indoor particles from urban centers of Guangzhou, China. *Sci. Total Environ.* **479**, 117–124. <https://doi.org/10.1016/j.scitotenv.2014.01.115> (2014).
- Haque, M. M., Sultana, S., Niloy, N. M., Quraishi, S. B. & Tareq, S. M. Source apportionment, ecological, and human health risks of toxic metals in road dust of densely populated capital and connected major highway of Bangladesh. *Environ. Sci. Pollut. Res.* **29** (25), 37218–37233. <https://doi.org/10.1007/s11356-021-18458-3> (2022).

15. Chu, H., Liu, Y., Xu, N. & Xu, J. Concentration, sources, influencing factors and hazards of heavy metals in indoor and outdoor dust: A review. *Environ. Chem. Lett.* **21** (2), 1203–1230. <https://doi.org/10.1007/s10311-022-01546-2> (2023).
16. Huang, C. C. et al. X. A comprehensive approach to quantify the source identification and human health risk assessment of toxic elements in park dust. *Environ. Geochem. Health.* **45** (8), 5813–5827. <https://doi.org/10.1007/s10653-023-01588-7> (2023).
17. Min, G. H. et al. Health risk assessment and source tracking of hazardous air pollutants in the Dalseong-gun industrial complex of Daegu. *J. Environ. Health Sci.* **51** (1), 29–37. <https://doi.org/10.5668/JEHS.2025.51.1.29> (2025).
18. Men, C. et al. Uncertainty analysis in source apportionment of heavy metals in road dust based on positive matrix factorization model and geographic information system. *Sci. Total Environ.* **652**, 27–39. <https://doi.org/10.1016/j.scitotenv.2018.10.212> (2019).
19. National Institute of Environmental Research. Environmental Health Assessment of Ondong Village Residents. (NIER, 2022).
20. ASTM International. Standard practice for collection of surface dust by micro-vacuum sampling for subsequent metals determination (ASTM D7144-05a). *ASTM Int.* (2003).
21. U.S. Environmental Protection Agency. Risk Assessment Guidance for Superfund. Vol. I. Human Health Evaluation Manual (Part E) (EPA/540/R-99/005) (U.S. EPA, 2004).
22. National Institute of Public Health and the Environment. *Human exposure to soil contamination: A qualitative and quantitative analysis towards proposals for human toxicological intervention values.* (RIVM, 1994).
23. National Institute of Environmental Research. *Korean Exposure Factors Handbook.* (NIER, 2019).
24. National Institute of Environmental Research. *Guidelines for Preparing Data on the Risks of Chemical Substances.* (NIER, 2021).
25. U.S. Environmental Protection Agency. Risk Assessment Guidance for Superfund. Vol. I. Human Health Evaluation Manual (Part A) (EPA/540/1-89/002). (U.S. EPA., 1989).
26. U.S. Environmental Protection Agency. *Soil Screening Guidance: User's Guide* (EPA/540/R-96/018). (U.S. EPA, 1996).
27. Min, G. H. et al. Assessment of heavy metal exposure levels (Pb, Hg, Cd) among South Koreans and contribution rates by exposure Route-Korean National Environmental Health Survey (KoNEHS) cycle 4 (2018~2020). *J. Environ. Health Sci.* **49** (5), 262–274. <https://doi.org/10.5668/JEHS.2023.49.5.262> (2023).
28. Pearson, K. L. I. I. On lines and planes of closest fit to systems of points in space. *Lond. Edinb. Phil. Mag J. Sci.* **2** (11), 559–572. <https://doi.org/10.1080/14786440109462720> (1901).
29. Kaiser, H. F. The application of electronic computers to factor analysis. *Educ. Psychol. Meas.* **20** (1), 41–151. <https://doi.org/10.1177/001316446002000116> (1960).
30. Liang, C. S. et al. Efficient data preprocessing, episode classification, and source apportionment of particle number concentrations. *Sci. Total Environ.* **744**, 140923. <https://doi.org/10.1016/j.scitotenv.2020.140923> (2020).
31. Statheropoulos, M., Vassiliadis, N. & Pappa, A. Principal component and canonical correlation analysis for examining air pollution and meteorological data. *Atmos. Environ.* **32** (6), 1087–1095. [https://doi.org/10.1016/S1352-2310\(97\)00377-4](https://doi.org/10.1016/S1352-2310(97)00377-4) (1998).
32. Park, J. et al. Source apportionment of PM_{2.5} in Seoul, South Korea and Beijing, China using dispersion normalized PMF. *Sci. Total Environ.* **833**, 155056. <https://doi.org/10.1016/j.scitotenv.2022.155056> (2022).
33. Székely, G. J. & Rizzo, M. L. A new test for multivariate normality. *J. Multivar. Anal.* **93** (1), 58–80. <https://doi.org/10.1016/j.jmva.2003.12.002> (2005).
34. Ward, J. R. Hierarchical grouping to optimize an objective function. *J. Am. Stat. Assoc.* **58** (301), 236–244. <https://doi.org/10.1080/01621459.1963.10500845> (1963).
35. Paatero, P., Eberly, S., Brown, S. G. & Norris, G. A. Methods for estimating uncertainty in factor analytic solutions. *Atmos. Meas. Techn.* **7** (3), 781–797. <https://doi.org/10.5194/amt-7-781-2014> (2014).
36. Kim, E., Hopke, P. K., Larson, T. V. & Covert, D. S. Analysis of ambient particle size distributions using unmix and positive matrix factorization. *Environ. Sci. Technol.* **38** (1), 202–209. <https://doi.org/10.1021/es030310s> (2004).
37. U.S. Environmental Protection Agency. *EPA Positive Matrix Factorization (PMF) 5.0 Fundamentals and User Guide* (EPA/600/R-14/108). (U.S. EPA, 2014).
38. Gaujoux, R. & Seoighe, C. A flexible R package for nonnegative matrix factorization. *BMC Bioinf.* **11**, 1–9 (2010). <http://www.biomedcentral.com/1471-2105/11/367>
39. Lee, D. D. & Seung, H. S. Learning the parts of objects by non-negative matrix factorization. *Nature* **401** (6755), 788–791. <https://doi.org/10.1038/44565> (1999).
40. Xie, J. P. & Ni, H. G. Chromatographic fingerprint similarity analysis for pollutant source identification. *Environ. Pollut.* **207**, 341–344. <https://doi.org/10.1016/j.envpol.2015.09.049> (2015).
41. Budisulistiorini, S. H. et al. Examining the effects of anthropogenic emissions on isoprene-derived secondary organic aerosol formation during the 2013 Southern oxidant and aerosol study (SOAS) at the Look Rock, Tennessee ground site. *Atmos. Chem. Phys.* **15** (15), 8871–8888. <https://doi.org/10.5194/acp-15-8871-2015> (2015).
42. Roy, A. et al. Heavy metal pollution in indoor dust of residential, commercial, and industrial areas: a review of evolutionary trends. *Air Qual. Atmos. Health.* **17** (4), 891–918. <https://doi.org/10.1007/s11869-023-01478-y> (2024).
43. Ali, M. U. et al. Compositional characteristics of black-carbon and nanoparticles in air-conditioner dust from an inhabitable industrial metropolis. *J. Clean. Prod.* **180**, 34–42. <https://doi.org/10.1016/j.jclepro.2018.01.161> (2018).
44. Min, G. H. et al. Health risk assessment and establishment of exposure limits for children and adults from heavy metals in indoor dust. *J. Environ. Health Sci.* **50** (5), 322–331. <https://doi.org/10.5668/JEHS.2024.50.5.322> (2024).
45. Calabrese, E. J., Priest, N. D. & Kozumbo, W. J. Thresholds for carcinogens. *Chem. Biol. Interact.* **341**, 109464. <https://doi.org/10.1016/j.cbi.2021.109464> (2021).
46. Devi, V. M. Sources and toxicological effects of some heavy metals—a mini review. *J. Toxicol. Stud.* **2** (1), 404–404. <https://doi.org/10.59400/jts.v2i1.404> (2024).
47. Halsband, C., Sørensen, L., Booth, A. M. & Herzke, D. Car tire crumb rubber: does leaching produce a toxic chemical cocktail in coastal marine systems? *Front. Environ. Sci.* **8**, 125. <https://doi.org/10.3389/fenvs.2020.00125> (2020).
48. Turner, A. & Filella, M. Hazardous metal additives in plastics and their environmental impacts. *Environ. Int.* **156**, 106622. <https://doi.org/10.1016/j.envint.2021.106622> (2021).
49. European Environment Agency. *EMEP/EEA Air Pollutant Emission Inventory Guidebook 2023* (EEA, 2023).
50. Brown, C. W., Goldfine, C. E., Allan-Blitz, L. T. & Erickson, T. B. Occupational, environmental, and toxicological health risks of mining metals for lithium-ion batteries: a narrative review of the pubmed database. *J. Occup. Med. Toxicol.* **19** (1), 35. <https://doi.org/10.1186/s12995-024-00433-6> (2024).
51. Hahldakis, J. N., Velis, C. A., Weber, R., Iacovidou, E. & Purnell, P. An overview of chemical additives present in plastics: Migration, release, fate and environmental impact during their use, disposal and recycling. *J. Hazard. Mater.* **344**, 179–199. <https://doi.org/10.1016/j.jhazmat.2017.10.014> (2018).
52. Norgate, T. E. & Rankin, W. J. Life cycle assessment of copper and nickel production. In *Proceedings of MINPREX 2000 International Congress on Mineral Processing and Extractive Metallurgy*, Carlton, Victoria, Australia. 133–138 (2000).
53. Zhang, J. et al. Emission characteristics of heavy metals from a typical copper smelting plant. *J. Hazard. Mater.* **424**, 127311. <https://doi.org/10.1016/j.jhazmat.2021.127311> (2022).
54. Lach, K. & Smolová, I. The emission of ultrafine particles in the manufacture of fireplace ceramic tiles. *Int. J. Environ. Impacts.* **2** (4), 325–335. <https://doi.org/10.2495/EI-V2-N4-325-335> (2019).
55. Minguiñón, M. C. et al. Air quality comparison between two European ceramic tile clusters. *Atmos. Environ.* **74**, 311–319. <https://doi.org/10.1016/j.atmosenv.2013.04.010> (2013).

Acknowledgements

Sincere thanks are extended by the authors to the Korea Environmental Industry & Technology Institute and the Ministry of Environment of the Republic of Korea for providing research grants through the Environmental Health Action Program, which made this study possible.

Author contributions

Details of each author with their contribution in this paper: Conceptualization, Data curation, Formal analysis, Investigation, Methodology, Resources, Software, Validation, Visualization, Writing original draft, Writing review & editing were performed by Gihong Min. Data curation, Formal analysis, Investigation, and Methodology were performed by Daehwan Kim, Jihun Shin, Youngtae Choe, and Sanghoon Lee. Writing original draft, Writing review & editing were performed by Jangwoo Lee, Kilyong Choi and Kyungwha Sung. Conceptualization, Data curation, Formal analysis, Funding acquisition, Investigation, Methodology, Project administration, Resources, Software, Supervision, Validation, Visualization, Writing original draft, Writing review & editing were performed by Wonho Yang. All authors read and approved the final manuscript. All the authors have seen and evaluated the manuscript and agreed to publish the same in the journal.

Funding

This work was supported by grants from the Korea Environmental Industry & Technology Institute through the Environmental Health Action Program funded by the Korea Ministry of Environment [Grant number RS-2021-KE002003].

Declarations

Competing interests

The authors declare no competing interests.

Ethics approval

This study was performed according to standard procedures after obtaining IRB approval from Daegu Catholic University (IRB No. CUIRB-2023-0054).

Consent to participate

Written informed consent for the collection of indoor settled dust samples was obtained from all participating households prior to sampling.

Additional information

Supplementary Information The online version contains supplementary material available at <https://doi.org/10.1038/s41598-025-23211-8>.

Correspondence and requests for materials should be addressed to W.Y.

Reprints and permissions information is available at www.nature.com/reprints.

Publisher's note Springer Nature remains neutral with regard to jurisdictional claims in published maps and institutional affiliations.

Open Access This article is licensed under a Creative Commons Attribution-NonCommercial-NoDerivatives 4.0 International License, which permits any non-commercial use, sharing, distribution and reproduction in any medium or format, as long as you give appropriate credit to the original author(s) and the source, provide a link to the Creative Commons licence, and indicate if you modified the licensed material. You do not have permission under this licence to share adapted material derived from this article or parts of it. The images or other third party material in this article are included in the article's Creative Commons licence, unless indicated otherwise in a credit line to the material. If material is not included in the article's Creative Commons licence and your intended use is not permitted by statutory regulation or exceeds the permitted use, you will need to obtain permission directly from the copyright holder. To view a copy of this licence, visit <http://creativecommons.org/licenses/by-nc-nd/4.0/>.

© The Author(s) 2025